Numerical Calculation of Pick-Up Coils Frequency Response as a Useful Tool for Local Magnetic Field Sensors Design

Nicolò Marconato and Matteo Bonotto

***Abstract*— The aim of this article is to present a useful numerical procedure suitable to accurately model pick-up probes for design-oriented purposes, reducing the required prototyping activity and allowing more accurate results with respect to analytic estimations, taking into account both inductive and capacitive effects in complex geometries. The proposed methodology is characterized by the following steps: 1) a partial element equivalent circuit (PEEC) formulation, speeded up by a parametric model order reduction (pMOR) technique, is used to efficiently model the probe in the frequency domain taking into account both inductive and capacitive effects; 2) a nonlinear least-squares solver is used to identify an equivalent *RLC* network describing the full behavior of the probe up to the first resonance frequency; and 3) a circuital model, considering the probe, the transmission line (TL), and the terminating impedance, is used to estimate the bandwidth of the complete system from the probe to the acquisition system. The experimental validation of the proposed method against the RFX-mod2 three-axis pick-up probe prototype is also presented, together with the application to the design of the magnetic sensors for the new Divertor tokamak test (DTT) facility.**

***Index Terms*— Frequency response, magnetic confinement fusion, magnetic diagnostic, parametric model order reduction (pMOR), partial element equivalent circuit (PEEC), three-axis pick-up probe.**

I. Introduction

THE inductive nature of pick-up coils implies high dynamic ranges and a broad bandwidth, features that make them widely used as local magnetic field sensors in any magnetic fusion device but must be adapted to specific constraints by an accurate design of coils and electronics. Once the probe effective area is defined by sensitivity requirements, thus determining the lower bound of the dynamic range, the specified upper bound is achieved by the proper design of the conditioning electronics. In principle, it is desirable to maximize the sensor bandwidth, but, on the other hand, it may be limited on purpose in order to control, in turn, the dynamic range [1].

It is well known that the frequency response of the coil is an essential feature of the sensor, which must be accurately determined [1]–[4]. Generally, it is experimentally obtained by a precise characterization [5], which needs an iterative prototypical activity. The opportunity to accurately know the frequency behavior of the coil in advance with a fast and efficient computational tool would make the design process of the whole sensor, from the probe to the signal acquisition chain, easier and more effective.

Usual numerical techniques, such as finite element methods, are not suitable for a precise frequency characterization of electrical systems on a wide frequency range, taking into account inductive and capacitive effects at the same time. This article describes our experience in the application of a code implementing the partial element equivalent circuit (PEEC) method for the numerical calculation of the frequency response of the pick-up sensors for the upgraded magnetic diagnostic system of the RFX-mod2 machine. The results have been validated by both code-code benchmarks and experimental data. The tool has then been routinely adopted for the design currently ongoing of the ex-vessel and in-vessel systems of local magnetic sensors of the DTT machine, significantly reducing the time and costs associated with the realization and characterization of prototypes.

This article is organized as follows. In Section II, the adopted methodology is described. In particular, the basic principles of the PEEC method and the general scheme of the pMOR technique are discussed in Section II-A. The equivalent network reproducing the frequency behavior of the probe is introduced in Section II-B. The circuit-oriented model of the whole acquisition chain is illustrated in Section II-C. In Section III, the application of the proposed method for the preliminary design of the magnetic sensors for the new Divertor Tokamak Test (DTT) facility is reported. Finally, conclusions are drawn in Section IV.

II. Methodology Description

This section is devoted to present a methodology for the development of an accurate model of a given pick-up coil for design-oriented purposes. The coil frequency response is an essential feature that influences the sensor performances and, thus, must be accurately determined. The steps of the procedure are described in the following.

Manuscript received 26 January 2022; revised 18 March 2022; accepted 9 April 2022. The review of this article was arranged by Senior Editor G. H. Neilson. *(Corresponding author: Nicolò Marconato.)*

Nicolò Marconato is with Consorzio RFX (CNR, ENEA, INFN, Università di Padova, Acciaierie Venete SpA), 35127 Padua, Italy, and also with the Dipartimento di Ingegneria Industriale (DII), Università di Padova, 35131 Padua, Italy (e-mail: nicolo.marconato@igi.cnr.it).

Matteo Bonotto is with Consorzio RFX (CNR, ENEA, INFN, Università di Padova, Acciaierie Venete SpA), 35127 Padua, Italy, and also with INFN-LNL, Viale dell'Università 2, 35020 Legnaro (Padua), Italy.

Color versions of one or more figures in this article are available at https://doi.org/10.1109/TPS.2022.3167854.

Digital Object Identifier 10.1109/TPS.2022.3167854

Fig. 1. RFX-mod2 three-axis pick-up probe prototype.

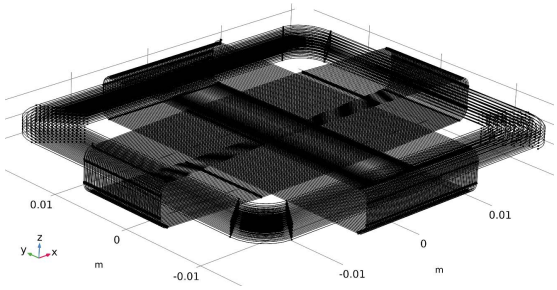

Fig. 2. Filamentary geometrical model of the RFX-mod2 three-axis pick-up coil windings used in the PEEC-MOR code.

In addition, the first essential step of this method was validated against the RFX-mod2 three-axis pick-up probe prototype (see Fig. 1). This pick-up coil is composed of three windings, one orthogonal to the other, to measure the three components of the magnetic field, wound on a Torlon[1] reel, high-performing polyamide-imide (PAI) [6].

A. PEEC Model of the Probe

A PEEC formulation for solving full-Maxwell's equations, with piecewise homogeneous and linear conductive, dielectric, and magnetic media, is used [7], [8]. This approach is based on the electric and magnetic field integral equations (EFIE and MFIE) in the frequency domain, with angular frequency ω

$$\boldsymbol{E}(\boldsymbol{r}) = -i\omega \boldsymbol{A}_e(\boldsymbol{r}) - \nabla\varphi_e(\boldsymbol{r}) - \frac{1}{\varepsilon_0}\nabla \times \boldsymbol{A}_m(\boldsymbol{r}) \tag{1}$$

$$\boldsymbol{H}(\boldsymbol{r}) = -i\omega \boldsymbol{A}_m(\boldsymbol{r}) - \nabla\varphi_m(\boldsymbol{r}) + \frac{1}{\mu_0}\nabla \times \boldsymbol{A}_e(\boldsymbol{r}) \tag{2}$$

where $\boldsymbol{E}$ is the electric field and $\boldsymbol{H}$ is the magnetic field. The potentials are given by their integral expressions functions of the volume electric and magnetic current and charge densities

$$\boldsymbol{A}_e(\boldsymbol{r}) = \mu_0 \int_\Omega \boldsymbol{J}(\boldsymbol{r}')g(\boldsymbol{r},\boldsymbol{r}')d\Omega \tag{3}$$

$$\boldsymbol{A}_m(\boldsymbol{r}) = \varepsilon_0 \int_\Omega \boldsymbol{J}_m(\boldsymbol{r}')g(\boldsymbol{r},\boldsymbol{r}')d\Omega \tag{4}$$

$$\varphi_e(\boldsymbol{r}) = \frac{1}{\varepsilon_0}\int_\Omega \rho_e(\boldsymbol{r}')g(\boldsymbol{r},\boldsymbol{r}')d\Omega \tag{5}$$

$$\varphi_m(\boldsymbol{r}) = \frac{1}{\mu_0}\int_\Omega \rho_m(\boldsymbol{r}')g(\boldsymbol{r},\boldsymbol{r}')d\Omega \tag{6}$$

where $\boldsymbol{J}$ and ρ_e are the conduction current density and the electric charge density, $\boldsymbol{J}_m$ and ρ_m are the magnetic current density and the magnetic charge density, and

$$g(\boldsymbol{r},\boldsymbol{r}') = \frac{1}{4\pi|\boldsymbol{r}-\boldsymbol{r}'|}. \tag{7}$$

The general PEEC formulation consists of the discretization of the field integral equations by piecewise constant pulse basis functions in order to extract an equivalent circuital representation of the modeled device [9]. The advantage is twofold: an accurate modeling of EM interactions in the air domain and a possible integration with external circuits. The particular implementation here adopted is based on the cell method, which, by using integral variables as problem unknowns, is naturally suited for developing circuit-like approaches, such as PEEC [7].

Like all integral formulations, the PEEC method gives rise to a linear system made up of dense matrices, whose number of nonzero elements grows with the square of the unknowns. Moreover, the analysis in the frequency domain, as it is of interest, in this case, requires the solution of the dense system as many times as a reasonable number of frequencies required to reconstruct the dynamic of the system. The high number of degrees of freedom (DoFs) required to develop accurate models, together with the high number of frequency evaluations, typically of the order of 10^2, needed to properly describe the frequency behavior, can be difficult to be handled from the computational point of view. To solve this problem, parametric model order reduction (pMOR) techniques can be adopted to speed up the calculation [10], reducing the required solutions of the system to a few units. The use of the pMOR approach allows for significantly reducing the computational complexity while substantially keeping the accuracy of the original solver. The adopted method is based on a classical proper orthogonal decomposition (POD) scheme [11], where the solution space is spanned in order to construct a proper basis that is used to project the problem according to a Galerkin scheme. The Gram–Schmidt orthogonalization is used to ensure a good condition number of the final equivalent parametric reduced-order model, whose solution can be performed very efficiently with a reduced memory requirement and very short computation time [12].

The PEEC formulation is of particular interest for our purposes because, being an integral method, it requires meshing only the conducting regions (i.e. the windings) and the dielectric media (i.e. the Torlon reel). Magnetic media are not considered in this problem. The filamentary geometry used to describe the three windings of the RFX-mod2 three-axis pick-up probe prototype can be seen in Fig. 2. Moreover, the PEEC method is suitable to be directly used to perform circuital simulations, such as the evaluation of the probe impedance in the frequency domain.

The frequency response of the probe was computed both with and without the Torlon reel and compared with the reference prototype response experimentally measured. In Fig. 3, the magnitude and phase of the calculated and measured impedance of the poloidal winding are reported. The effect on the frequency behavior of the impedance due to the

[1]Registered Trademark.

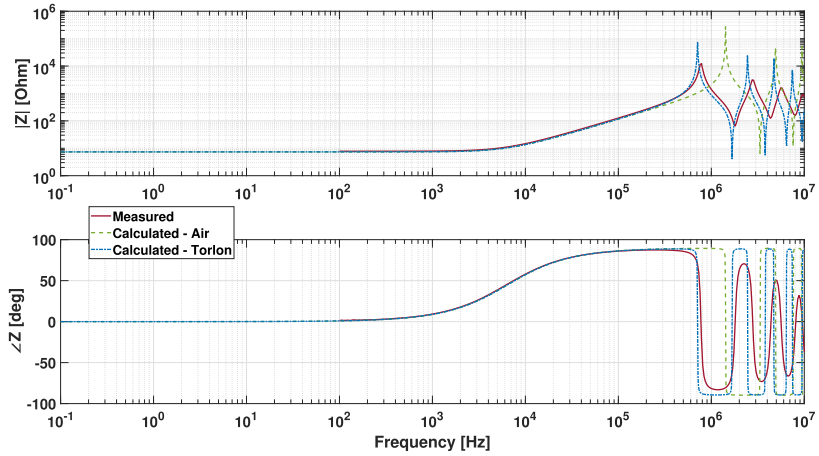

Fig. 3. Magnitude (top) and phase (bottom) of the impedance of the poloidal winding of the RFX-mod2 three-axis pick-up probe as a function of frequency. Dashed green: calculated response of the air coil. Dashed-dotted blue: calculated response of the coil with Torlon reel. Continuous red: experimental data.

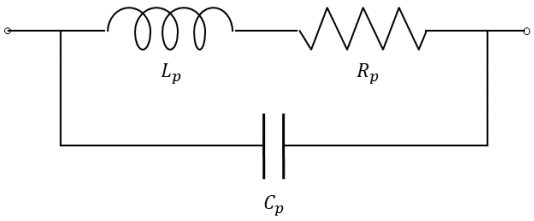

Fig. 4. RLC network used to model the frequency response of the real probe.

Torlon reel is clear, as it considerably increases the capacitive contribution; as a consequence, the main resonance frequency is considerably lower. Moreover, it increases the losses in the high-frequency part, however without affecting the probe's operating range.

B. Equivalent RLC Network Identification

A simple RLC network is then used as an equivalent circuit to model the frequency response of the real probe. The RLC network used in this activity is shown in Fig. 4. Indeed, it is well known [3] that a typical measured frequency response already in the range up to few kHz cannot be reduced to a simple first-order transfer function, and the equivalent probe circuit must include also the capacitance contribution.

Actually, an even more complex equivalent network would be necessary in order to correctly reproduce the high-frequency behavior. Since, for practical purposes, reproducing the frequency response up to the first resonance frequency is enough, the simple RLC circuit shown in Fig. 4 is able to correctly model the probe in the frequency range of interest. Once the frequency dependence of the probe impedance $\dot{Z}(f)$ is obtained with the accurate PEEC model, the RLC parameters are identified fitting, by means of a nonlinear least-squares method (i.e. MATLAB trust-region-reflective algorithm), the following equivalent impedance:

$$\dot{Z}_{\mathrm{eq}}(f) = \frac{R - i\left(wR^2C + w^3L^2C - wL\right)}{1 + w^2\left(R^2C^2 - 2LC\right) + w^4L^2C^2}. \qquad (8)$$

TABLE I
MEASURED VERSUS ESTIMATED RLC NETWORK PARAMETERS

	measured	estimated	Δ
$R[\Omega]$	8.04	7.4	8%
$L[\mu\mathrm{H}]$	170.5	182.3	7%
$C[\mathrm{pF}]$	246.8	274.3	11%

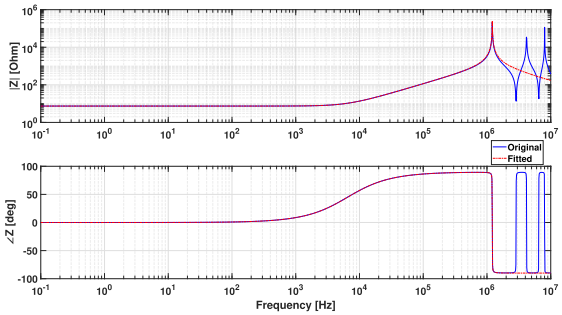

Fig. 5. Magnitude (top) and phase (bottom) of the impedance of the accurate PEEC-MOR model (solid blue) and the RLC equivalent network (dashed-dotted red) as a function of the frequency.

It is worth noting that the best results have been obtained by fitting the only impedance phase. Fig. 5 shows the comparison between the amplitude and phase of the impedance as a function of the frequency of the original PEEC model and the identified equivalent network, showing a satisfactory accuracy in the frequency range of interest for the application.

The RLC parameters of the equivalent network of the RFX-mod2 three-axis pick-up probe prototype have been experimentally measured by an HP-4194A impedance analyzer. The comparison between estimated and measured parameters of the poloidal winding can be seen in Table I.

C. Complete Circuit Model (From Probe to Electronics)

The RLC equivalent network describing the probe, obtained at the previous step, is integrated into a SPICE-like circuit model to account also the transmission line (TL) from the probe to the acquisition system and the terminating impedance.

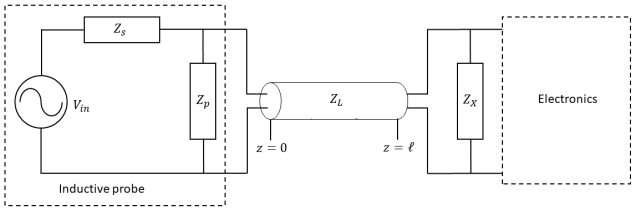

Fig. 6. Schematic view of the complete circuit model from the probe to the acquisition system.

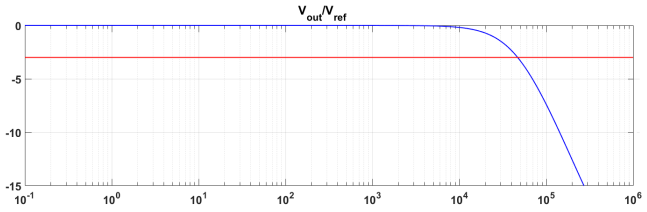

Fig. 7. Signal $V_{\text{out}}/V_{\text{ref}}$ (blue) as a function of frequency. The bandwidth at -3 dB is also highlighted.

The scheme of this model is shown in Fig. 6, where, specifically:

1) a linear inductor with self-inductance L_p subject to an electromotive force V_{in} linked to the measured magnetic flux;
2) the probe internal resistance R_p and self-capacitance C_p;
3) a TL of impedance Z_L, which generally connects the probes directly to the electronics input stage;
4) a terminating impedance Z_X, normally smaller than the electronics input impedance, connected in parallel to improve the frequency response.

It can be observed that the probe is described by means of the equivalent network presented in the previous paragraph, once the ideal voltage generator has electromotive force $V_{\text{in}} = 0$.

This stage of the analysis is required to estimate the bandwidth of the complete system. In case the bandwidth does not fulfill the design requirements, the probe geometry and characteristics can be adequately tuned in order to fulfill such constraints. This approach clearly allows reducing significantly the time and costs associated with the realization and characterization of prototypes.

Fig. 7 shows the overall frequency response $V_{\text{out}}/V_{\text{in}}$ (blue), together with the -3-dB level (red). The intersection of the two corresponds to the cutoff frequency limiting the sensor bandwidth. Here, V_{out} is the signal measured by the acquisition system, and V_{in} is the ideal electromotive force induced in the probe, neglecting all the parasitic elements. For lower frequency ranges, such a ratio is $\approx$1, being the effects of C_p and Z_L negligible. The more the frequency increases, the more such parasitic effects are prominent, provoking a strong attenuation of the signal. For the case of the RFX-mod2 three-axis pick-up probe, the bandwidth of the system probe and TL is of the order of 50 kHz. The length of the TL used in this simulation is 30 m. The line assumes a propagation velocity of $1.67 \cdot 10^8$ m/s and a characteristic impedance of 98 Ω. The line was terminated with a 100-Ω resistor.

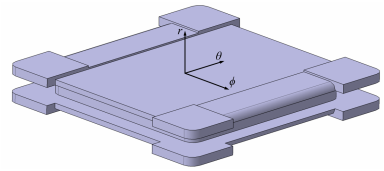

Fig. 8. Draft CAD model of the DTT ex-vessel three-axis probe: overall dimensions are 70 $\times$ 70 $\times$ 10 mm.

TABLE II
GEOMETRICAL PARAMETERS OF THE DTT EX-VESSEL POLOIDAL WINDING

Φ_{cab} [mm]	0.2	0.25	0.3
$Turn\ N\#$	400	320	266
A_{eff} [m^2]	0.212	0.17	0.141

III. DESIGN OF DTT MAGNETIC SENSORS

The primary aim of the DTT facility is to explore alternative power exhaust solutions for DEMO since conventional divertor based on detached conditions, to be tested on the ITER device, cannot be extrapolated to a fusion reactor [13]. This new experimental facility will be located in Frascati, Italy, and is presently in its design phase.

The proposed procedure is being currently used for the design of DTT magnetic sensors. Thanks to the peculiar features of the PEEC model, it is possible, at this preliminary stage, to investigate the effect of the reel dimension and material, and the conductor diameters.

The following is an example of an analysis of these factors applied to the poloidal (similar results apply to the toroidal one) and radial winding of the ex-vessel three-axis probe foreseen for DTT. These probes will be installed on the outer surface of the vacuum vessel, between the vessel and the cryostat, where the maximum available dimensions are 70 $\times$ 70 mm wide and 10 mm thick. A Torlon or ceramic reel will be adopted, depending on the final decision on the vessel baking temperature. A draft CAD model of the reel is reported in Fig. 8.

A. Results for the Poloidal Winding

The reel material influences the coil response as the permittivity of the material changes and, thus, the capacitive contribution. The cable diameter instead has a geometric effect, implying a different number of winding turns and cable length, for given reel dimensions. Three different cable diameters have been tested, and the related data of the poloidal winding, in terms of turn number and effective area, are summarized in Table II.

In Fig. 9, the frequency behavior of the poloidal winding impedance with 0.25-mm cable diameter when a Torlon reel, a Macor reel, and without reel are computed by means of the full PEEC model is compared.

The effect of the conductor diameter on the frequency behavior of the impedance, also evaluated with the full PEEC model, is instead reported in Fig. 10. It can be seen that a small variation on the diameter of the conductor winding, without varying the geometry of the winding itself, results in a considerable variation of the frequency response, as highlighted by the fact that the first resonance is shifted from

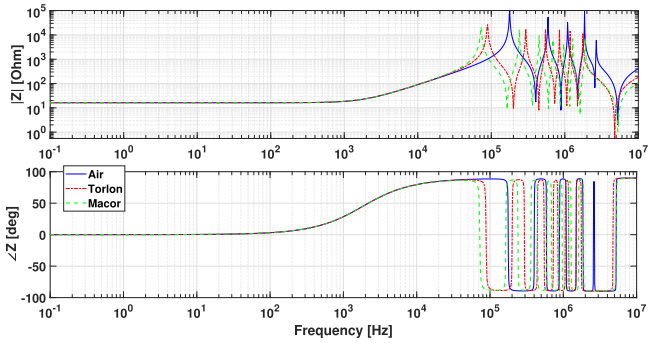

Fig. 9. Magnitude (top) and phase (bottom) of the impedance of the poloidal winding as a function of the frequency, with and without the supporting reel and 0.25-mm cable diameter: without reel solid blue, with Torlon reel in dashed red, and with Macor reel in dashed-dotted green lines.

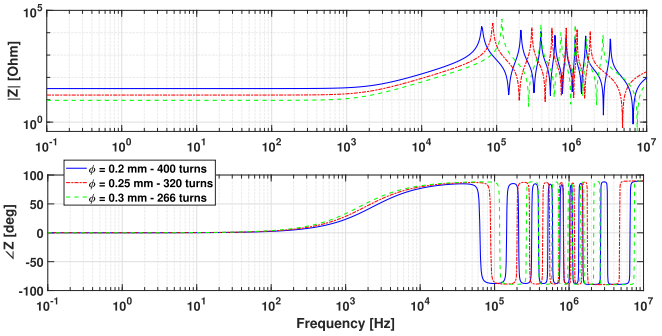

Fig. 10. Magnitude (top) and phase (bottom) of the impedance of the poloidal winding as a function of the frequency with Torlon reel and for three values of the cable diameter: 0.2 mm diameter in solid blue, 0.25 mm diameter in dashed red, and 0.3 mm diameter in dashed-dotted greed lines.

TABLE III

IDENTIFIED *RLC* PARAMETERS FOR DIFFERENT ANALYZED CASES FOR THE DTT EX-VESSEL COIL POLOIDAL WINDING

Material	Φ_{cab} [mm]	$R[\Omega]$	L [mH]	C [nF]
Torlon	0.2	31.65	2.17	2.89
Air	0.25	16.24	1.38	0.58
Torlon	0.25	16.24	1.4	2.31
Macor	0.25	16.24	1.4	3.44
Torlon	0.3	9.39	0.97	1.9

≈270 kHz to more than 400 kHz. The main reason is the increased number of turns (50% more) when reducing the diameter from 0.3 to 0.2 mm.

In Table III, the identified *RLC* parameters of the equivalent network representing the probe are reported for different analyzed cases. The accuracy of this approach, for these cases, is the same of the previous case presented in Section II-B for RFX-mod2 probes. These parameters have then been used to calculate the comprehensive frequency response of the whole system with the model described in Section II-C. The results for the different cable diameters considered and for three different TL lengths (30, 60, and 100 m), when the Torlon reel is adopted, are summarized in Fig. 11.

The figure clearly shows that the contribution of the TL dominates over the effect of the probe cable diameter in the definition of the global frequency response. These results were obtained by terminating the TL with a snubber made up of a 50-nF capacitor in series to a 500-Ω resistor, in order to suppress the main resonance peak, affecting as little as possible

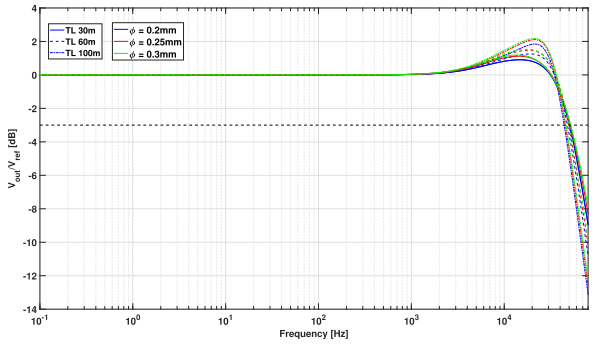

Fig. 11. Frequency response of the whole poloidal sensor acquisition chain for the different cable diameters and TL lengths analyzed with Torlon reel. The simulated frequency limit corresponds to the frequency up to which the equivalent *RLC* network is accurate.

TABLE IV

GEOMETRICAL PARAMETERS OF THE DTT EX-VESSEL COIL RADIAL WINDING

Φ_{cab} [mm]	0.2	0.25	0.3
$Turn\ N\#$	750	400	320
A_{eff} [m^2]	2.41	1.89	1.56

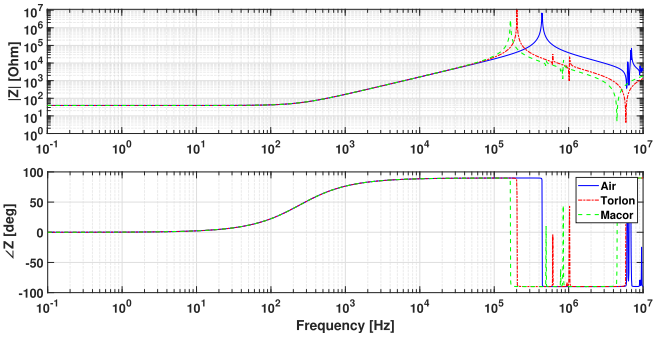

Fig. 12. Magnitude (top) and phase (bottom) of the impedance of the radial winding as a function of the frequency, with and without the supporting reel and 0.25-mm cable diameter: without reel solid blue, with Torlon reel in dashed red, and with Macor reel in dashed-dotted green lines.

the lower frequency range. An adjustment of this one and the addition of a second snubber, in order to dump also the secondary peaks, can be operated in a final design phase.

B. Results for the Radial Winding

The same analysis has been carried out for the radial winding of the ex-vessel probe. The geometric data, again for the three cable diameters, are summarized in Table IV.

The effect on the frequency behavior of the impedance of the reel material and the conductor diameter is also evaluated considering the full PEEC model and is shown in Figs. 12 and 13 respectively.

The *RLC* parameters of the equivalent network of Fig. 4 for the proposed configurations are reported in Table V. Finally, the whole frequency response of the system (i.e. radial probe and signal line) is computed for the different cable diameters, and the three TL lengths considered, when the Torlon reel is adopted, are reported in Fig. 14.

The figure clearly shows that, in the case of the radial winding, the contribution of the probe cable diameter dominates

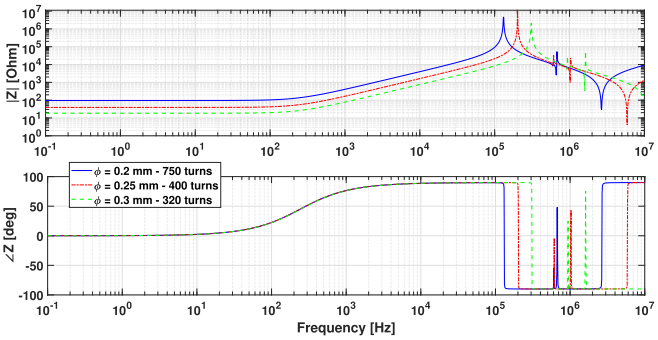

Fig. 13. Magnitude (top) and phase (bottom) of the impedance of the radial winding as a function of the frequency, with Torlon reel and for three values of the cable diameter: 0.2 mm diameter in solid blue, 0.25 mm diameter in dashed red, and 0.3 mm diameter in dashed-dotted greed lines.

TABLE V
IDENTIFIED *RLC* PARAMETERS FOR DIFFERENT ANALYZED CASES FOR THE DTT EX-VESSEL COIL RADIAL WINDING

Material	Φ_{cab} [mm]	$R[\Omega]$	L [mH]	C [pF]
Torlon	0.2	95.77	63	23.4
Air	0.25	39.14	26	5
Torlon	0.25	39.14	26	23.4
Macor	0.25	39.14	26	35.6
Torlon	0.3	18.51	11	23.3

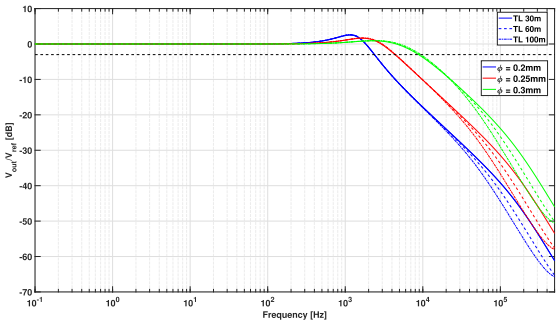

Fig. 14. Frequency response of the whole radial sensor acquisition chain for the different cases analyzed. Simulated frequency limit corresponds to the frequency up to which the equivalent RLC network is accurate.

over the TL length in the definition of the global frequency response, moving from a band of about 2.5 kHz in the case of 0.2-mm cable diameter to a frequency of about 9 kHz with $\phi = 0.3$ mm. The snubber terminating the TL in this analysis is made up of a 200-nF capacitor in series to a 500-Ω resistor.

It is worth noting that all these analyses on the DTT sensors are very preliminary, carried out especially to arrange the procedure. For instance, the large effective area of the radial winding, required to measure small fields outside the vessel, will necessarily be reduced to widen the frequency band.

IV. CONCLUSION

An integrated numerical procedure with the aim of estimating the frequency response of inductive magnetic field probes, comprehensive of the whole acquisition chain from the probe to the electronics, has been developed and successfully benchmarked with the RFXmod2 pick-up probe prototype. A PEEC approach, an integral formulation for full-wave analysis, is adopted for modeling the probe. The tool integrates a parametric model order reduction (pMOR) technique, which allows considerably speeding up the calculation and, thus, fast testing of several cases. The capability to efficiently take into account also the capacitive effect is one of the strengths of the PEEC approach.

The advantages of this modeling activity are clear, allowing to significantly reduce the time and costs associated with the realization and characterization of prototypes.

Interestingly, the analysis showed that nonmetallic coil supports also limit the frequency band due to their significant contribution to capacitive effects.

It is worth noting that the use of PEEC formulation would allow modeling the complete system without the need for external SPICE-like solvers. However, the adopted approach resulted in a more flexible solution for the particular application to magnetic probe design optimization.

REFERENCES

[1] N. Marconato, R. Cavazzana, P. Bettini, and A. Rigoni, "Accurate magnetic sensor system integrated design," *Sensors*, vol. 20, no. 10, p. 2929, May 2020, doi: 10.3390/s20102929.

[2] E. J. Strait, "Magnetic diagnostic system of the DIII-D tokamak," *Rev. Sci. Instrum.*, vol. 77, no. 2, Feb. 2006, Art. no. 023502, doi: 10.1063/1.2166493.

[3] J.-M. Moret, F. Buhlmann, D. Fasel, F. Hofmann, and G. Tonetti, "Magnetic measurements on the TCV tokamak," *Rev. Sci. Instrum.*, vol. 69, no. 6, pp. 2333–2348, Jun. 1998, doi: 10.1063/1.1148940.

[4] E. J. Strait, E. D. Fredrickson, J.-M. Moret, and M. Takechi, "Chapter 2: Magnetic diagnostics," *Fusion Sci. Technol.*, vol. 53, no. 2, pp. 304–334, Feb. 2008, doi: 10.13182/FST08-A1674.

[5] J. G. Bak, S. G. Lee, and D. Son, "Performance of the magnetic sensor and the integrator for the KSTAR magnetic diagnostics," *Rev. Sci. Instrum.*, vol. 75, no. 10, pp. 4305–4307, Oct. 2004, doi: 10.1063/1.1789620.

[6] N. Marconato *et al.*, "Design of the new electromagnetic measurement system for RFX-mod upgrade," *Fusion Eng. Des.*, vol. 146, pp. 906–909, Sep. 2019, doi: 10.1016/j.fusengdes.2019.01.110.

[7] R. Torchio, P. Alotto, P. Bettini, D. Voltolina, and F. Moro, "A 3-D PEEC formulation based on the cell method for full-wave analyses with conductive, dielectric, and magnetic media," *IEEE Trans. Magn.*, vol. 54, no. 3, pp. 1–4, Mar. 2018, doi: 10.1109/TMAG.2017.2750319.

[8] R. Torchio, F. Moro, G. Meunier, J.-M. Guichon, and O. Chadebec, "An extension of unstructured-PEEC method to magnetic media," *IEEE Trans. Magn.*, vol. 55, no. 6, pp. 1–4, Jun. 2019, doi: 10.1109/TMAG.2018.2889435.

[9] A. E. Ruehli, "Inductance calculations in a complex integrated circuit environment," *IBM J. Res. Develop.*, vol. 16, no. 5, pp. 470–481, Sep. 1972.

[10] R. Torchio, A. Arduino, L. Zilberti, and O. Bottauscio, "A fast tool for the parametric analysis of human body exposed to LF electromagnetic fields in biomedical applications," *Comput. Methods Programs Biomed.*, vol. 214, Feb. 2022, Art. no. 106543, doi: 10.1016/j.cmpb.2021.106543.

[11] P. Benner, K. Willcox, and S. Gugercin, "A survey of projection-based model reduction methods for parametric dynamical systems," *SIAM J. Sci. Comput.*, vol. 57, no. 4, pp. 483–531, 2011, doi: 10.1137/130932715.

[12] G. Rozza, D. B. P. Huynh, and A. T. Patera, "Reduced basis approximation and a posteriori error estimation for affinely parametrized elliptic coercive partial differential equations," *Arch. Comput. Methods Eng.*, vol. 15, no. 3, pp. 229–275, Sep. 2008, doi: 10.1007/s11831-008-9019-9.

[13] R. Albanese and A. Pizzuto, "The DTT proposal. A tokamak facility to address exhaust challenges for DEMO: Introduction and executive summary," *Fusion Eng. Design*, vol. 122, pp. 274–284, Nov. 2017, doi: 10.1016/j.fusengdes.2016.12.030.

Open Access funding provided by 'Università degli Studi di Padova' within the CRUI CARE Agreement